Available online at www.sciencedirect.com
SCIENCE DIRECT
Journal of Photochemistry and Photobiology A: Chemistry 178 (2006) 264–270
Journal of Photochemistry and Photobiology A:Chemistry
www.elsevier.com/locate/jphotochem

Quantum dynamics of exciton recurrence motion in dendritic molecular aggregates

Hiroya Nitta [a,*], Mitsuo Shoji [a], Masahiro Takahata [a], Masayoshi Nakano [b], Daisuke Yamaki [c], Kizashi Yamaguchi [a]

[a] *Department of Chemistry, Graduate School of Science, Osaka University, Machikaneyama 1-1, Toyonaka, Osaka 560-0043, Japan*
[b] *Division of Chemical Engineering, Department of Materials Engineering Science, Graduate School of Engineering Science, Osaka University, Toyonaka, Osaka 560-8531, Japan*
[c] *Graduate School of Information Science, Nagoya University, Chigusa-ku, Nagoya 464-8601, Japan*

Available online 7 December 2005

Abstract

The quantum master equation approach involving weak exciton–phonon coupling has been applied to the investigation of the exciton recurrence motion in molecular aggregate models with dendritic structures. Each monomer in the models is assumed to be a dipole unit (a two-state monomer) coupled with each other by the dipole–dipole interaction. Two types of the dendritic molecular aggregates, which have mutually different interactions through the branching points, are examined. A generation of one-exciton states by an electric field and its subsequent exciton dynamics with and without relaxation terms have been investigated. It is found that the configuration of each dipole unit significantly affects the coherent motions of the exciton population. We also suggest the possibility of controlling the coherent exciton motions by tuning the frequency of an external electric field.

Keywords: Quantum dynamics; Exciton; Recurrence motion; Molecular aggregates; Coherence; Quantum beat

1. Introduction

Energy transfer is one of the most fundamental processes in chemistry. Dendrimers with fractal dimensions are known to show the efficient excitation energy transfer from the external to the central regions [1–3]. Such molecules have ordered geometries and well-directed energy gradients between the peripheral and the core regions. It has also revealed that the relaxation effect is important for the directional energy migration, i.e. population relaxation [4,5]. Because the population relaxation also contributes to the phase relaxation, such energy migration is an incoherent process. Recently, coherent processes have attracted much attention in relation to developments of quantum molecular devices [6–8] by the use of spin and pseudo spins, such as exciton. For example, coherent superposition of the excited states generated by optical method causes a recurrence motion of the excitation between constituent units in molecular systems.

Hochstrasser and co-workers [9,10] have investigated the coherent excitation energy transfer between two-identical chromophores (2,2′-binaphthyl, BN) in solution, and have found a damped oscillation corresponding to exciton recurrence associated with the interaction energy ($\Delta = 41\ \mathrm{cm}^{-1}$) and the dephasing time (T_2') of 0.2 ps. Wynne and Hochstrasser [11] have presented a theoretical framework for the coherent energy transfer in solution and have applied it to the analysis of their experiments.

Yamazaki et al. have investigated the intramolecular energy transfer of various anthracene dimers, e.g. dianthrylbenzene (DAB) and dithiaanthracenophane (DTA) groups (Fig. 1), in solution [12–14]. The fluorescence anisotropy decay of these molecules displays the oscillatory behavior originated from the recurrence motion of an excitation between two anthracenes. This suggests that the intramolecular energy transfer proceeds coherently in these systems. Generally, it is very difficult to observe such oscillatory signals because of the rapid dephasing by solvent molecules and of the difficulty in detecting the fluorescence signals from a mate of the dimer selectively. Yamazaki et al. have concluded that the relatively rigid molecular structures of DAB and DTA are key factors in detecting the quantum

* Corresponding author. Tel.: +81 6 6850 5405; fax: +81 6 6850 5550.
E-mail address: hnitta@chem.sci.osaka-u.ac.jp (H. Nitta).

1010-6030/$ – see front matter © 2005 Elsevier B.V. All rights reserved.
doi:10.1016/j.jphotochem.2005.10.040

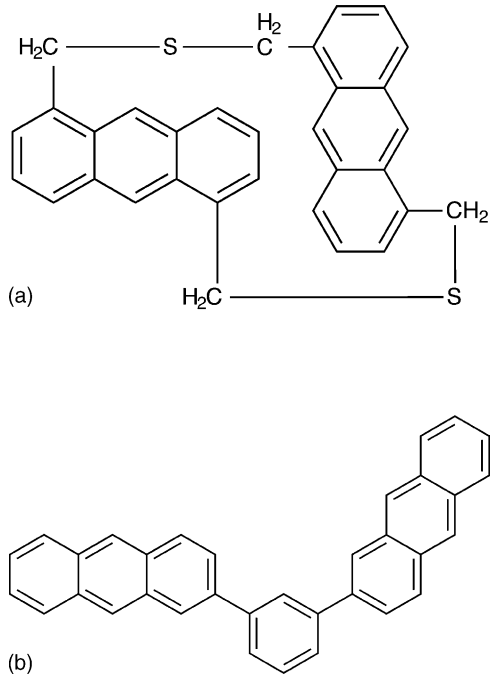

Fig. 1. Molecular structures of (a) DTA and (b) DAB.

beat of fluorescence anisotropy decay. They have pointed out that the longer dephasing time in DTA (1.0 ps) can be explained by the less flexible and more rigid conformation than that in BN (0.2 ps).

Previously, we have performed theoretical investigations of energy migration in dendrimers on the basis of the quantum master equation [15,16]. As a continuation of previous work, we here focus on the coherent process, such as recurrence motion of excitons in dendritic systems using two types of molecular aggregate structures. One is an aggregate modeled after the real extended phenylacetylene dendrimers [1–3] (see Fig. 2b), while the other one is a different aggregate model with significant interactions between neighboring monomers through the branching points (see Fig. 2c). Such difference in modeling is expected to cause variations in the energetics and also the coherent dynamics of exciton population. A possibility of controlling the coherent exciton motions by tuning the frequency of an external field is also examined. Implications of the computational results are discussed in relation to importance of aggregate structures for less decoherence rule.

2. Methods

2.1. Model Hamiltonians

We consider molecular aggregate systems composed of two-state monomers $\{i\}$ with the excitation energy $\{E_i\}$ and the dipole moment $\{\mu_i\}$ ($i = 1, 2, \ldots, N$; N is the number of monomers). Interactions between i- and j-th monomers are assumed to be represented by the dipole–dipole interaction J_{ij}. This approximation is considered to be valid when the intermolecular distance R is larger than the size of a monomer. The

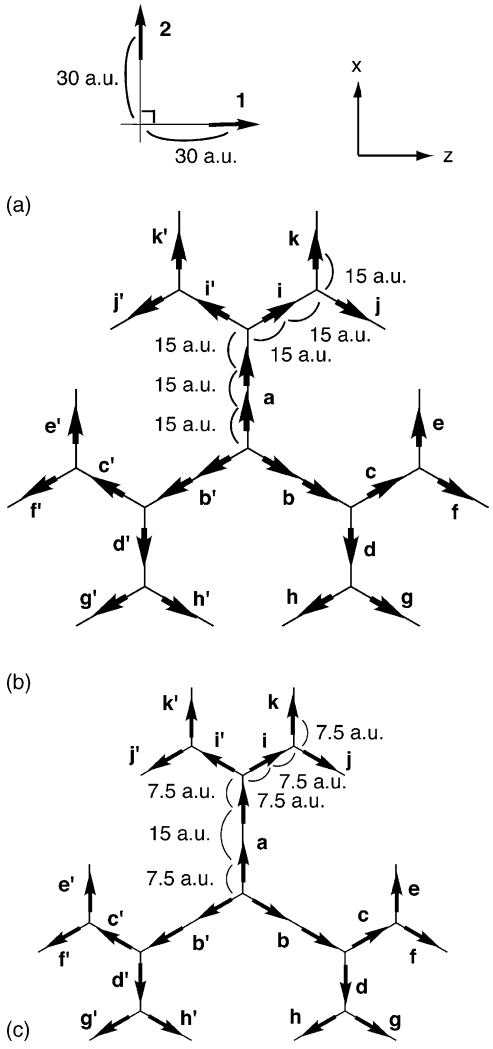

Fig. 2. Structures and labeling of the models used in this paper: (a) dimer model, (b) dendritic model I and (c) dendritic model II. Each two-state monomer dipole unit is represented by an arrow. For the dendritic models I and II, the angle between neighboring linear legs at all branching points is assumed to be 120°.

Hamiltonian for the aggregate system is expressed by

$$H_s = \sum_i^N E_i |i\rangle\langle i| + \frac{1}{2}\sum_{i\neq j}^N J_{ij}|i\rangle\langle j|, \tag{1}$$

where

$$J_{ij} = \frac{1}{4\pi\varepsilon_0 R_{ij}^3}\mu_i\mu_j\{\cos(\theta_{i_j} - \theta_{j_i}) - 3\cos\theta_{i_j}\cos\theta_{j_i}\}. \tag{2}$$

Here, $|i\rangle$ is the aggregate basis, which means that the i-th monomer is excited, and R_{ij} is the intermolecular distance between i- and j-th monomers. $\theta_{i_j}(\theta_{j_i})$ is the angle between the dipole moment of $i(j)$-th monomer and the vector drawn from i-th monomer to j-th monomer.

In the one-exciton approximation, aggregate system is described in the eigenstates $\{|\psi_k\rangle\}$ with energies $\{\omega_k\}$. We obtain $|\psi_k\rangle$ and ω_k by solving the following eigenvalue equation

$$H_S|\psi_k\rangle = \omega_k|\psi_k\rangle, \tag{3}$$

where

$$|\psi_k\rangle = \sum_i^N |i\rangle\langle i|\psi_k\rangle = \sum_i^N C_{ki}|i\rangle \tag{4}$$

Here, $\{|\psi_k\rangle, k=2, 3, \ldots, N+1\}$ denote the one-exciton states, and $|\psi_1\rangle$ represents the ground state. An exciton on the i-th monomer interacts with nuclear vibrations, which are approximately described by the phonon Hamiltonian H_R:

$$H_R = \sum_i \sum_{q_i} \Omega_{q_i} c_{i,q_i}^+ c_{i,q_i}, \tag{5}$$

where Ω_{q_i} is the frequency of the phonon in the state q_i associated with i-th monomer, and c_{i,q_i}^+ and c_{i,q_i} are the creation and annihilation operators of phonon in the state q_i, respectively. The interaction Hamiltonian between exciton and phonon is given by

$$H_{SR} = \sum_i \sum_{q_i} |i\rangle\langle i|(\kappa_{i,q_i}^* c_{i,q_i}^+ + \kappa_{i,q_i} c_{i,q_i}), \tag{6}$$

where κ_{i,q_i} is a coupling constant between the exciton $|i\rangle$ and a phonon state $|q_i\rangle$.

2.2. Master equation

Total Hamiltonian is given by

$$H = H_0 + H_{SR}, \tag{7}$$

where H_0 is the static Hamiltonian:

$$H_0 = H_S + H_R. \tag{8}$$

The time evolution of the aggregate system under the Born–Markov approximation [17] is represented by

$$\frac{d}{dt}\tilde{\rho}(t) = -\int_0^t dt' \, \mathrm{tr}_R[\tilde{H}_{SR}(t), [\tilde{H}_{SR}(t'), \tilde{\rho}(t)R_0]], \tag{9}$$

where ρ is the reduced density operator, for the aggregate system, and the tilde denotes the interaction picture. R_0 is the density operator for the phonon system. From Eq. (9), the time evolution of the density matrix elements in the Schrödinger picture is given by

$$\frac{d}{dt}\rho_{\alpha\beta} = \langle\psi_\alpha|\frac{d\rho}{dt}|\psi_\beta\rangle = -i(\omega_\alpha - \omega_\beta)\rho_{\alpha\beta} - \sum_{mn} \Gamma_{\alpha\beta;mn}\rho_{mn} - F(t)\sum_n (\mu_{\alpha n}\rho_{n\beta} - \rho_{\alpha n}\mu_{n\beta}), \tag{10}$$

where the contribution from electric field is added in the third term; $F(t)$ is a time dependent external electric field, and μ_{mn} is a transition moment from state m to n. The relaxation term Γ is given by

$$\Gamma_{\alpha\beta;mn} = \sum_k \sum_i [\delta_{\beta n} C_{\alpha i}^* |C_{ki}|^2 C_{mi}\gamma_i(\omega_m - \omega_k) + \delta_{\alpha m} C_{ni}^* |C_{ki}|^2 C_{\beta i}\gamma_i(\omega_n - \omega_k)] - \sum_i [C_{\alpha i}^* C_{mi} C_{ni}^* \times C_{\beta i}\{\gamma_i(\omega_m - \omega_\alpha) + \gamma_i(\omega_n - \omega_\beta)\}] \tag{11}$$

and

$$\gamma_i(\omega) = \frac{2\gamma_i^0}{1 + \exp(-\omega/k_B T)}, \tag{12}$$

which is determined from the thermal equilibrium condition [18]. In Eq. (12), γ_i^0 indicates the high temperature limit of $\gamma_i(\omega)$, and k_B is the Boltzmann constant. We numerically solve Eq. (10) by the sixth-order Runge–Kutta method. The density matrix elements in the aggregate basis $|i\rangle$ at time t are calculated by

$$\rho_{ii}(t) = \sum_{\alpha\beta} C_{\alpha i}\rho_{\alpha\beta}(t)C_{\beta i}^* \tag{13}$$

3. Results and discussion

3.1. Exciton states of the aggregate models

We consider three aggregate models: a dimer model (Fig. 2a), dendritic models I (Fig. 2b) and II (Fig. 2c). Each arrow represents a dipole unit (a two-state monomer). The dimer model is the simplest case to observe the recurrence motion of exciton population between two monomers. For the dimer model, the transition energy E and the transition moment μ of the monomers are assumed to be 38,000 cm^{-1} and 8D [15], respectively. By diagonalizing of Hamiltonian H_S, we obtain two one-exciton states with energies: $\omega_2 = 37957.3\ cm^{-1}$ and $\omega_3 = 38042.7\ cm^{-1}$. These states are nearly degenerate ($\Delta\omega = 85.4\ cm^{-1}$), so that they can be excited coherently by light.

For both dendritic systems I (Fig. 2b) and II (Fig. 2c), all the dipole units are identical: their transition energy and transition moment are assumed to be 38,000 cm^{-1} and 5D, respectively. Model I possesses slight interactions between adjacent legs at the branching points because their intermolecular distance ($15\sqrt{3}$ a.u.) is larger than that in the same leg region (15 a.u.). In contrast, model II possesses significant interactions between adjacent legs at the branching points because the intermolecular distances among monomers in such legs ($7.5\sqrt{3}$ a.u.) are comparable to those in the same leg regions (15 a.u.). After the diagonalization of the aggregate Hamiltonian H_S, the transition energies and the magnitudes of transition moments between the ground and the one-exciton states are obtained as shown in Fig. 3. Multi-step one-exciton states are found for both aggregates though some differences in the energy gaps are observed for these multi-states with significant transition moments. It is also found that the exciton states with significant transition moments tend to lie below the transition energy of the constituent monomers (38,000 cm^{-1}), and the energies of one-exciton states with significant large transition moments in model II are lower than those in model I. These features have already been elucidated by J- and H-aggregate type interactions [5].

The exciton distributions in one-exciton states with large transition moments for models I and II are shown in Fig. 4. States 2 and 3, states 6 and 7, and states 9 and 10 for model I are degenerate in transition energy, respectively, while states 2 and 3, states 5 and 6, states 9 and 10, and states 11 and 12 for model

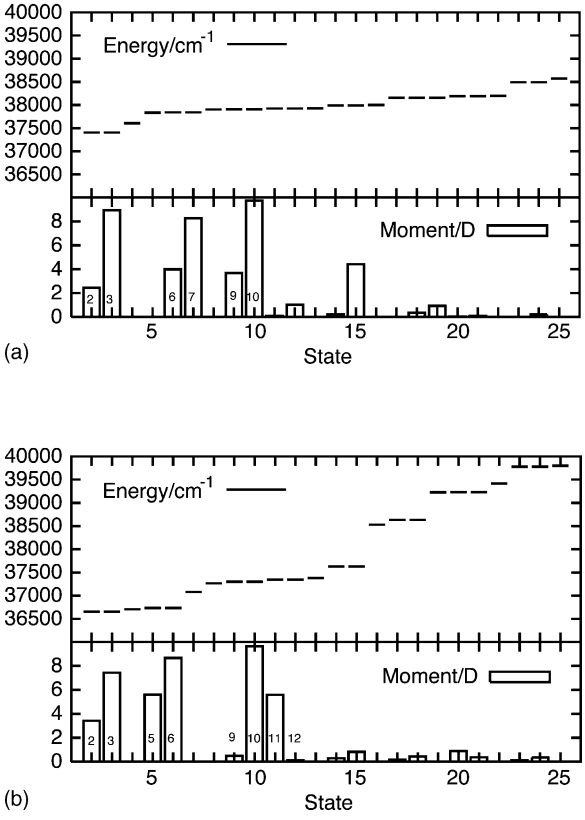

Fig. 3. Calculated transition energies (cm^{-1}) and the magnitude of transition moments [D] for the dendritic model I (a) and model II (b) shown in Fig. 2.

II are degenerate in transition energy, respectively. The exciton distribution of the degenerate state (11, 12) for model II is similar to that of the state (9, 10) though their phase relation is different from each other. It is noted that the exciton in state (2, 3) for model I is well localized in the internal region, while that for model II is distributed not only in the internal region but also in some parts of intermediate region. Also, for model I, the significant energy gaps have been observed between states (2, 3) and (6, 7), while for model II, they are observed between states (5, 6) and (9, 10). These differences are predicted to originate in the difference between interactions at the branching points of two models. Nearly degenerate states are found in both models: $\Delta\omega = 66.2\,cm^{-1}$ between states (6, 7) and (9, 10) for model I, and $\Delta\omega = 80.6\,cm^{-1}$ between states (2, 3) and (5, 6) and $\Delta\omega = 42.8\,cm^{-1}$ between states (9, 10) and (11, 12) for model II. Hence, these states can be excited coherently by laser light.

3.2. Exciton dynamics

The exciton dynamics is performed using Eqs. (10)–(12). The power of the applied electric field and the temperature T are fixed to be $100\,MW/cm^2$ and 300 K, respectively, throughout this paper. The frequencies of the field are resonant with specific exciton states, which have large transition moments. The polarization axis of the field is fixed to be parallel with the x-axis as shown in Fig. 2.

Fig. 5 shows the exciton population dynamics for the dimer model after the irradiation of 300 optical cycles (ca. 263 fs). In Eq. (12), γ^0 values, which are the high temperature limit ($T = \infty$) of $\gamma(\omega)$, for both monomers are assumed to be $10\,cm^{-1}$. The oscillation of the exciton population between two monomers (quantum beat) is confirmed, the feature of which implies that states (2) and (3) are excited coherently. Oscillation period is estimated to be about 400 fs, which corresponds to the energy difference between states (2) and (3) ($85.4\,cm^{-1}$). Although our calculation does not take into account the effect of the damping from the excited to the ground state, the relaxation effect between

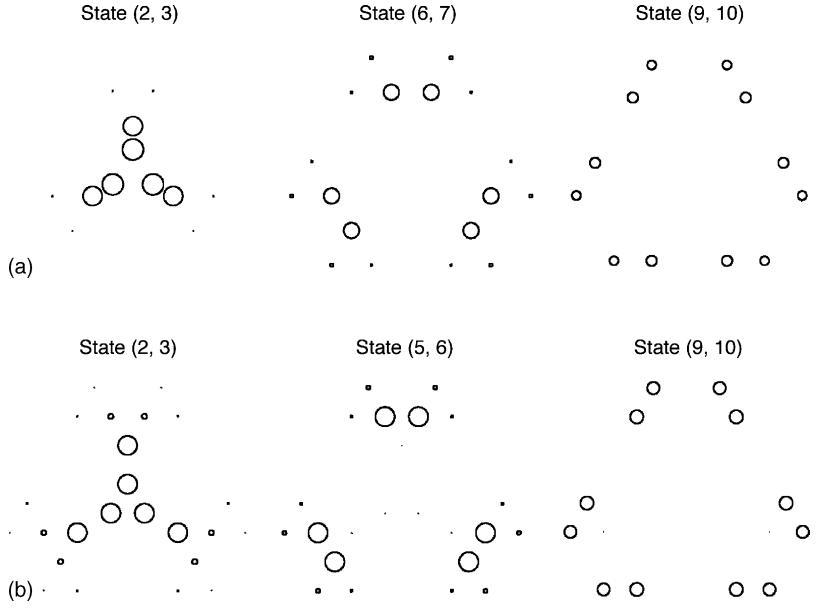

Fig. 4. Spatial distributions of one-exciton in degenerate; (a) states 2 and 3, states 6 and 7, and states 9 and 10 for model I; (b) states 2 and 3, states 5 and 6, and states 9 and 10 for model II. The size of circle indicates the magnitude of the exciton distribution.

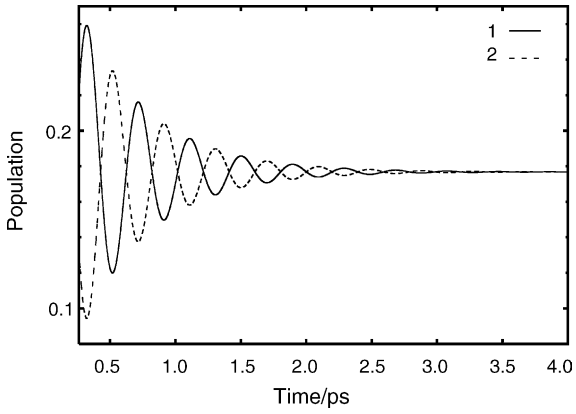

Fig. 5. Time-evolution of the exciton population in dimer model (Fig. 2a) after the irradiation of the external field. The variation of exciton population is shown in monomer unit. Labels 1 and 2 correspond to those in Fig. 2a.

exciton states described by the term $\Gamma\rho$ in Eq. (10) appears in the damped oscillation of the exciton populations.

In order to reveal the effect of the differences in structure and energetics of the dendritic models I and II, we first perform the exciton dynamics without relaxation terms. The $\gamma(\omega)$ value at the high temperature limit γ^0 for all monomers is assumed to be 0 cm^{-1} (non-relaxation), and the applied electric field is resonant with the exciton state (10, 9) for models I ($\omega = 37908.5\,cm^{-1}$) and state (10, 9) for model II ($\omega = 37301.7\,cm^{-1}$). These fields generate the superposition state composed of states (10, 9) and (7, 6) for model I, and the superposition state composed of states (10, 9) and (11, 12) for model II. Fig. 6a and b show the calculated results for models I and II, respectively. The electric fields are turned off after the irradiation of 300 optical cycles; ca. 264 fs for model I and ca. 268 fs for model II, respectively.

Though Fig. 6a and b show that the exciton populations of these models are almost localized in the external region, the recurrence motions of the exciton populations among monomers are significantly different between models I and II. Primary, recurrence motions occur between monomers **e**(**e**′) and **f**(**f**′), between monomers **j**(**j**′) and **k**(**k**′), and between monomers **c**(**c**′) and **d**(**d**′) for model I as shown in Fig. 6a. In contrast, for model II, recurrence motions occur between monomer pairs **g**(**g**′)–**h**(**h**′) and **j**(**j**′)–**k**(**k**′) as shown in Fig. 6b. These differences can be understood from the exction distributions of the states which compose the superposition state: states (6, 7) and (9, 10) for model I, and states (9, 10) and (11, 12) for model II. For model I, each segmented region (**e**(**e**′) and **f**(**f**′), **j**(**j**′) and **k**(**k**′), and **c**(**c**′) and **d**(**d**′)) is isolated from other region because of the weak interaction through the branching points. Hence, the oscillations of the exciton population are well localized in each segmented region. It is found for model II that the exciton populations on the monomer pairs **e**(**e**′)–**f**(**f**′) are slightly oscillating. This behavior implies the recurrence motion of excitation between monomer pairs **g**(**g**′)–**h**(**h**′) and **j**(**j**′)–**k**(**k**′) through the monomer pairs **e**(**e**′)–**f**(**f**′).

Next, we consider the exciton dynamics with the relaxation terms. The $\gamma(\omega)$ values at the high temperature limit γ^0 for all monomers are assumed to be 10 cm^{-1}, and the frequencies of the applied fields and the irradiation period are identical to those

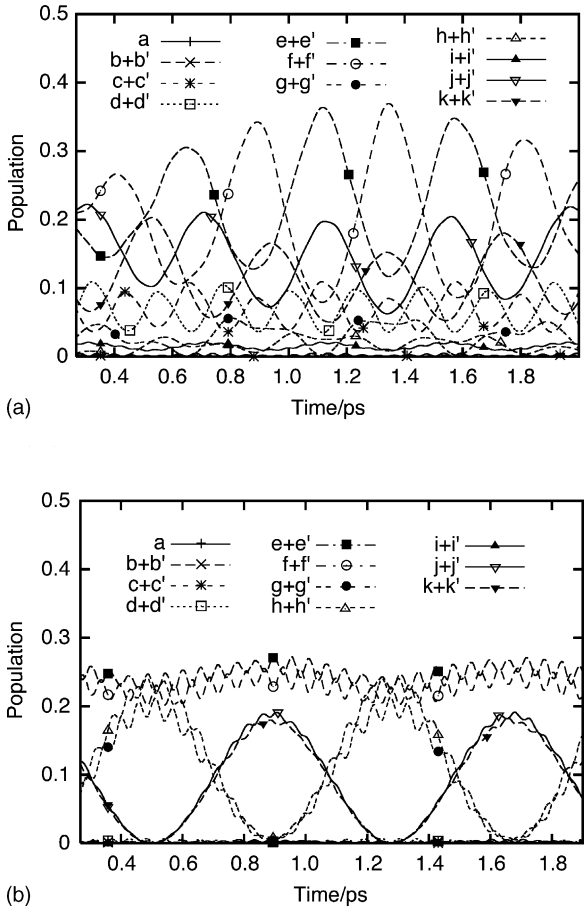

Fig. 6. Time-evolution of the exciton population at each monomer without relaxation terms for the dendritic models I (a) (Fig. 2b) and II (b) (Fig. 2c) after the irradiation of the external field. Monomer labels (**a**, **b**(**b**′), . . ., **k**(**k**′)) correspond to those in Fig. 2b and c. The frequency of the external field is resonant with the state (10, 9) of each model.

of non-relaxation case. Fig. 7a and b show the obtained results for models I and II, respectively. The exciton coherent motions similar to those in the non-relaxation case are found for both models. The relaxation causes the suppression of the oscillation amplitude of the exciton recurrence motions, as well as the exciton migration from the external region to the intermediate and the internal regions.

3.3. Control of the exciton coherent motion

The dendritic model II has two groups of nearly degenerate states: states (2, 3)–(5, 6) and states (9, 10)–(11, 12), which are well separated from each other in transition energy. This suggests that model II can be used to generate a superposition state that is different from those in Figs. 6b and 7b by the external field. The frequency of the electric field is set to be resonant with the state (5, 6) ($\omega = 36732.9\,cm^{-1}$) in order to examine the coherent motion of the exciton population generated by this field. The time evolution of the exciton population is shown in Fig. 8a and b, which represent the non-relaxation ($\gamma^0 = 0\,cm^{-1}$) and the relaxation ($\gamma^0 = 10\,cm^{-1}$) cases, respectively. The external field is turned off after the irradiation of 300 optical cycles

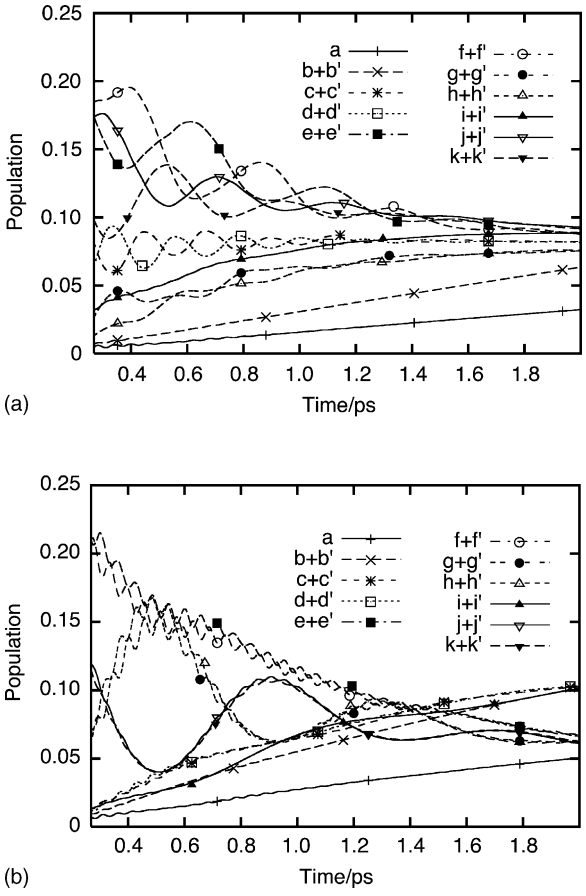

Fig. 7. Time-evolution of exciton population at each monomer with relaxation terms for the dendritic models I (a) (Fig. 2b) and II (b) (Fig. 2c) after the irradiation of the external field. Monomer labels (**a**, **b**(**b**′), . . ., **k**(**k**′)) correspond to those in Fig. 2b and c. The frequency of the external field is resonant with the state (10, 9) of each model.

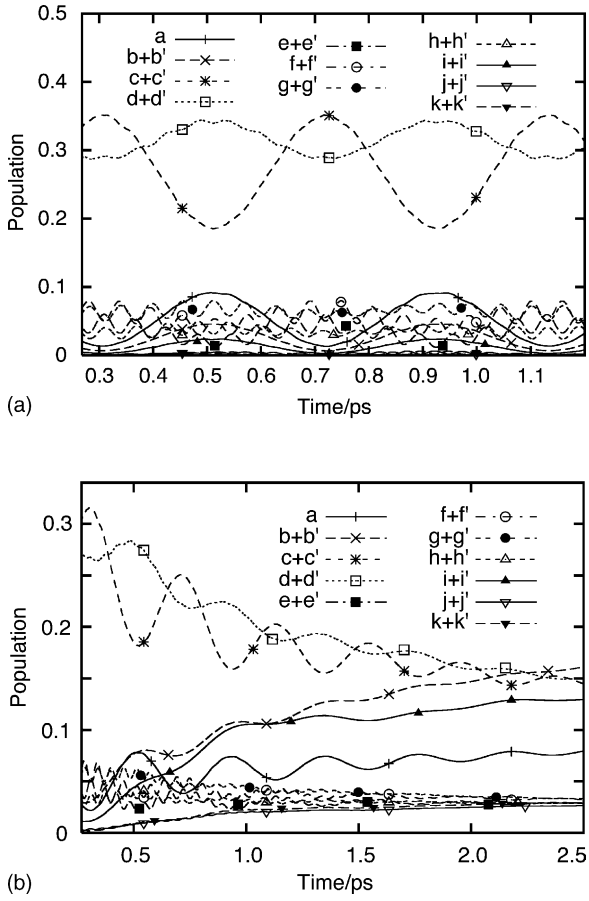

Fig. 8. Time-evolution of exciton population at each monomer for the dendritic model II (Fig. 2c) after the irradiation of the external field: non-relaxation case (a) and relaxation case (b). Monomer labels (**a**, **b**(**b**′), . . ., **k**(**k**′)) correspond to those in Fig. 2c. The field is resonant with state (5, 6) shown in Fig. 4b.

(ca. 272 fs). Fig. 8a shows the oscillatory behavior of exciton population, which differs from that shown in Fig. 6b. The exciton recurrence motions are mainly found between the regions **c**(**c**′) and **i**(**i**′)–**a**–**b**(**b**′)–**d**(**d**′). This is predicted to be related to the exciton distributions of states (2, 3) and (5, 6). Under this condition, the exciton oscillation is shown to occur through the branching points. Namely, in the relaxation case, exciton migration with oscillatory behavior is predicted to occur from the intermediate to the internal regions (Fig. 8b).

From the above results, it is concluded for model II that the exciton population shows two types of the oscillatory behaviors, which correspond to the superposition states composed of states (2, 3) and (5, 6) and those of states (9, 10) and (11, 12), respectively. The former one shows the exciton motions along the branches of the dendritic linear-legs, originating in the superposition states composed of states (2, 3) and (5, 6), the exciton of which is distributed in the internal and the intermediate regions. In contrast, the latter one shows the half-circular motion of the exciton population originated from the superposition of states (9, 10) and (11, 12), the exciton of which is distributed in the outermost regions. Such behaviors of exciton motion can be controlled by adjusting the frequency of the external electric field to the excitation energy creating superposition states with desired distribution regions for exciton recurrence motion. The present result suggests the possibility of controlling the coherent motions of the exciton in molecular aggregates with dendritic architecture. Therefore, derivation of less decoherence rule for quantum phase control is an interesting future problem.

4. Conclusion

We have applied the master equation approach involving weak exciton–phonon coupling [15,16] to the investigation of the exciton coherent motion. It is found that the configuration of the aggregate structure significantly affects the coherent dynamics of the exciton population as well as the energetics of the aggregate system. Also, we have revealed a possibility of controlling the exciton recurrence motion in dendritic molecular aggregates by changing the configuration of each dipole unit and/or adjusting the external field frequency.

Acknowledgments

One of the authors (K.Y.) thanks Professor Iwao Yamazaki for his continuous encouragement suggestions, and discussions for our theoretical studies on molecular systems. We would like to

dedicate this paper for the special issue in honor of his retirement from Hokkaido University.

References

[1] C. Devadoss, P. Bharathi, J.S. Moore, J. Am. Chem. Soc. 118 (1996) 9635–9644.
[2] R. Koplemam, M. Shortreed, Z.-Y. Shi, W. Tan, Z. Xu, J.S. Moore, A. Bar-Haim, J. Klafter, Phys. Rev. Lett. 78 (1997) 1239–1242.
[3] V.D. Kleiman, J.S. Melinger, D. McMorrow, J. Phys. Chem. B105 (2001) 5595–5598.
[4] K. Harigaya, Chem. Phys. Lett. 29 (1999) 33–36.
[5] M. Nakano, M. Takahata, H. Fujita, S. Kiribayashi, K. Yamaguchi, Chem. Phys. Lett. 323 (2000) 249–256.
[6] K. Yamaguchi, M. Nakano, H. Nagao, M. Okumura, S. Yamanaka, T. Kawakami, D. Yamaki, M. Nishino, Y. Shigeta, K. Kitagawa, Y. Takano, M. Takahata, R. Takeda, Bull. Korean Chem. Soc. 24 (2003) 864–880.
[7] M. Takahata, M. Shoji, S. Yamanaka, M. Nakano, K. Yamaguchi, Polyhedron 24 (2005) 2653–2657.
[8] M. Takahata, M. Shoji, H. Nitta, R. Takeda, S. Yamanaka, M. Okumura, M. Nakano, K. Yamaguchi, Int. J. Quantum Chem. 105 (2005) 615–627.
[9] Y.R. Kim, P. Share, M. Pereira, M. Sarisky, R.M. Hochstrasser, J. Chem. Phys. 91 (1989) 7557–7562.
[10] F. Zhu, C. Galli, R.M. Hochstrasser, J. Chem. Phys. 98 (1993) 1042–1057.
[11] K. Wynne, R.M. Hochstrasser, J. Raman Spectrosc. 26 (1995) 561–569.
[12] I. Yamazaki, S. Akimoto, N. Aratani, A. Osuka, Bull. Chem. Soc. Jpn. 77 (2004) 1959–1971.
[13] I. Yamazaki, N. Aratani, S. Akimoto, T. Yamazaki, A. Osuka, J. Am. Chem. Soc. 125 (2003) 7192–7193.
[14] I. Yamazaki, S. Akimoto, T. Yamazaki, S.-I. Sato, Y. Sakata, J. Phys. Chem. A106 (2002) 2122–2128.
[15] M. Takahata, M. Nakano, H. Fujita, K. Yamaguchi, Chem. Phys. Lett. 363 (2002) 422–428.
[16] M. Takahata, M. Nakano, K. Yamaguchi, J. Theor. Comput. Chem. 2 (2003) 459–479.
[17] H.J. Carmichael, Statistical Methods in Quantum Optics, vol. 1, Springer–Verlag, Berlin, 1999.
[18] J.A. Leegwater, J.R. Durrant, D.R. Klug, J. Phys. Chem. B101 (1997) 7205–7210.